INTERNATIONAL JOURNAL OF CIRCUIT THEORY AND APPLICATIONS
Int. J. Circ. Theor. Appl. 2012; **40**:777–792
Published online 23 January 2011 in Wiley Online Library (wileyonlinelibrary.com). DOI: 10.1002/cta.755

Harmonic balance-based control of a boost DC/AC converter

Josep M. Olm[1, 2, *, †], Domingo Biel[2], Mario Spinetti-Rivera[3] and Enric Fossas[4, 5]

[1]*Department of Applied Mathematics IV, Universitat Politècnica de Catalunya, Vilanova i la Geltrú, Spain*
[2]*Institute of Industrial and Control Engineering, Universitat Politècnica de Catalunya, Barcelona, Spain*
[3]*School of Engineering, Universidad de Los Andes, Mèrida, Venezuela*
[4]*Institute of Industrial and Control Engineering, Universitat Politècnica de Catalunya, Barcelona, Spain*
[5]*Department of Automatic Control, Universitat Politécnica de Catalunya, Barcelona, Spain*

SUMMARY

The achievement of step-up inversion with a boost DC/AC converter requires appropriate periodic references for inductor currents, which have to satisfy ordinary differential equations (ODE) of the Abel type. These are equations with highly unstable solutions for which the existence of periodic solutions remains unproved. Hence, the studies reported so far in this subject obtain periodic output voltages that approximately track the expected profile using different periodic current references that do not exactly satisfy the Abel ODE. However, neither an explanation of why are periodic output voltages still obtained, nor an assessment of the output voltage error is provided. This paper analyzes the effect of using periodic current references in a Lyapunov-based controlled boost DC/AC converter performing step-up inversion tasks. It is shown that, for sufficiently accurate current references, the system exhibits asymptotically stable periodic solutions with bounded error. Moreover, the paper propounds the use of Harmonic Balance (HB)-based techniques to obtain such current references. Simulation and experimental results confirm that this choice yields periodic output voltages with an error that may be lowered using higher HB approximations. Copyright © 2011 John Wiley & Sons, Ltd.

Received 10 March 2010; Revised 5 August 2010; Accepted 21 November 2010

KEY WORDS: step-up inversion; boost DC/AC converter; Lyapunov-based control; Harmonic Balance

1. INTRODUCTION

Uninterruptible power supply devices or ac power sources are key elements of power conditioning systems. They are designed to supply an ac load from a dc source [1–3]. Usually, the power stage circuits in charge of performing DC/AC conversion are based on a full-bridge buck switching converter topology. When ac amplitudes higher than the dc input voltage are required, the classical design combines a step-up turns ratio transformer and a buck converter in the DC/AC conversion circuit. However, this approach entails some drawbacks related to the transformer nonidealities (leakage inductances, limited bandwidth, etc.) and increases the weight and size of the converter circuit. The boost DC/AC converter does not show these problems and can perform DC/AC step-up conversion.

One of the main issues when facing step-up inversion with a boost DC/AC converter is the obtention of bounded, periodic references for the inductor currents. This is due to the fact that such signals should satisfy a nonlinear ODE of the Abel type [4] for which not only there is no way of obtaining an analytical solution, but also it is not actually known whether it has periodic

*Correspondence to: Josep M. Olm, Department of Applied Mathematics IV, Universitat Politècnica de Catalunya, Vilanova i la Geltrú, Spain.
†E-mail: josep.olm@upc.edu

solutions. Indeed, to the authors' knowledge, the already reported existence results for periodic solutions of these ODE are only applicable to DC tracking [5, 6], and not to pure inversion.

Hence, the existing literature dealing with this subject considers different periodic current references that do not satisfy the Abel ODE. The proposal in [7] uses a double loop control, namely, an inductor current control inner loop and an output voltage control outer loop. A feedforward control technique is also applied to improve the system robustness in front of external disturbances. The controllers are designed by using the known time-decoupling between the inductor and capacitor dynamics. The paper does not present any theoretical analysis which validates the time-decoupling and may help the designer in control parameter tuning. The paper compares the results with those obtained by using the sliding mode proposal of [8]. The sliding mode scheme considers the inductor current and the capacitor voltage errors as feedback variables. The inductor current error is obtained by high-pass filtering the inductor current, which assumes that the inductor current is always close to its reference. This hypothesis yields some problems in transient response, as stated in the experimental comparison discussed in [7]. Sliding mode control is also used in [9], where a double loop sliding mode is designed to track sinusoidal signals in a boost inverter. The inductor current reference is obtained as the output of a Proportional-Integral (PI) controller of the capacitor voltage. A novel perspective can be found in [10], where a passive-based control design is applied to guarantee state asymptotic convergence to the reference values. As in [9], the current reference is obtained as the output of a PI voltage controller and presents the same drawback, namely that the overall stability remains unproved. The proposals in [11, 12] use an energy shaping control strategy that allows the obtention of a stable limit cycle which produces a pre-specified oscillating behavior for currents and voltages under known and unknown resistive loads, respectively. In both cases the current reference is approximated by a first harmonic signal. No analysis of the effect of using such current reference approximations in the output voltage is carried out.

This paper studies the tracking of a sinusoidal reference by the differential load of a Lyapunov-based controlled boost DC/AC inverter. By posing the problem in terms of a periodic system affected by a periodic perturbation that appears because the selected periodic current references do not exactly meet the Abel ODE, it is first proved that if the perturbation term is small enough, then the closed-loop system responds with an asymptotically stable periodic solution. Moreover, the difference between such a solution and reference currents and voltages vector is shown to be of the same order as the disturbance term.

Harmonic Balance (HB) has been long used to improve the accuracy of the theoretical predictions in the analysis of power converters (see, for example [13, 14]) based on averaged models. This paper also proposes the use of the HB method to compute current reference approximations that approximately satisfy the specific Abel ODE. In case the HB approximations exist and converge, the output voltage error is expected to tend to zero. Otherwise, an alternative technique is to use ideal, first-order HB approximations, which are always obtainable and have an analytical, closed-form expression that depends explicitly on the converter parameters. The drawback of this latter approach is an amplitude difference with the expected output voltage, which can be tackled by an appropriate tuning of the control law parameters at the cost of slight Total Harmonic Distortion (THD) increasing. The study is validated by means of both simulation and experimental results.

The remainder of the paper is organized as follows. Section 2 studies the tracking of periodic references by a boost DC/AC inverter. Section 3 introduces an HB-based technique that provides periodic current references for the inductor currents. Sections 4 and 5 contain, respectively, simulation and experimental results. Finally, conclusions and further research lines are summarized in Section 6.

2. MATHEMATICAL ANALYSIS

Throughout the paper, $\|\cdot\|$ denotes the uniform norm, i.e. $\|\cdot\| = \|\cdot\|_\infty$, while $\|\cdot\|_2$ stands for the euclidean 2-norm.

The boost DC/AC converter, depicted in Figure 1, consists of two identical boost converters connected in opposition and sharing the output resistance. The system dynamics may be modelled

DOI: 10.1002/cta

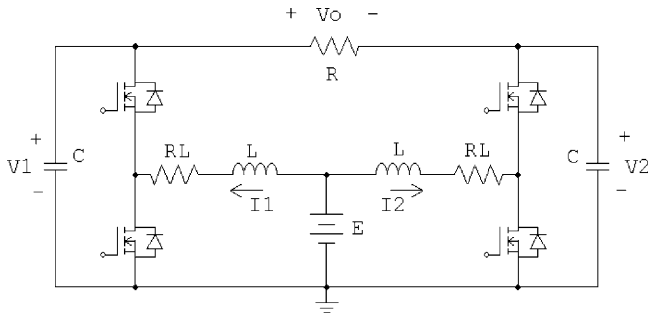

Figure 1. Boost DC/AC converter.

selecting the inductance currents and output voltages $I_1(\tau)$, $V_1(\tau)$, $I_2(\tau)$, $V_2(\tau)$ as state variables. Then, using Kirchhoff's laws

$$\begin{aligned}
\dot{I}_1 &= (E - R_L I_1 - u_1 V_1) L^{-1}, \\
\dot{V}_1 &= -(V_1 - V_2)(RC)^{-1} + u_1 I_1 C^{-1}, \\
\dot{I}_2 &= (E - R_L I_2 - u_2 V_2) L^{-1}, \\
\dot{V}_2 &= -(V_2 - V_1)(RC)^{-1} + u_2 I_2 C^{-1},
\end{aligned} \tag{1}$$

where the derivatives are calculated with respect to the time variable τ and the control actions u_1, u_2 take values in the discrete set $\{0, 1\}$. Notice that the control signal u_1 is associated to the half bridge of the left side of circuit depicted in Figure 1, whereas u_2 is related to the half bridge drawn on the right side. The branch switches operate in complementary mode, that is, $u_i = 1$ when its corresponding upper switch is conducting, while $u_i = 0$ when the corresponding lower switch is on.

The goal is to make the output voltage $V_o(\tau) = V_1(\tau) - V_2(\tau)$ track a pure sinusoidal signal

$$\bar{V}_o(\tau) = V_a \sin 2\pi v \tau.$$

This will be achieved forcing $V_1(\tau)$ and $V_2(\tau)$ to track appropriate offset DC signals, i.e.

$$\bar{V}_i(\tau) = V_{of} + (-1)^{i+1} \frac{V_a}{2} \sin 2\pi v \tau, \quad i = 1, 2, \tag{2}$$

with $V_{of} - |V_a|/2 > E > 0$.

For a systematic analysis it is advisable to work with a dimensionless system equivalent to Equation (1) and exhibiting a minimum number of parameters. Hence, with the change of variables

$$x_1 = \frac{1}{E}\sqrt{\frac{L}{C}} I_1, \quad x_2 = \frac{V_1}{E}, \quad x_3 = \frac{1}{E}\sqrt{\frac{L}{C}} I_2, \quad x_4 = \frac{V_2}{E}, \quad t = \frac{1}{\sqrt{LC}} \tau$$

and the introduction of the new parameters

$$\lambda = \frac{1}{R}\sqrt{\frac{L}{C}}, \quad \lambda_L = R_L \sqrt{\frac{C}{L}}, \tag{3}$$

(1) may be written as:

$$\begin{aligned}
\dot{x}_1 &= 1 - \lambda_L x_1 - u_1 x_2, \\
\dot{x}_2 &= -\lambda(x_2 - x_4) + u_1 x_1, \\
\dot{x}_3 &= 1 - \lambda_L x_3 - u_2 x_4, \\
\dot{x}_4 &= -\lambda(x_4 - x_2) + u_2 x_3,
\end{aligned} \tag{4}$$

where the derivatives are now calculated with respect to t.

DOI: 10.1002/cta

The change of variables makes the voltage references to be

$$\begin{aligned}\bar{x}_i(t) &= a+(-1)^{\frac{i}{2}+1}\frac{b}{2}\sin\omega t, \quad i=2,4,\\ \bar{x}_o(t) &= x_2(t)-x_4(t)=b\sin\omega t,\end{aligned} \tag{5}$$

where $a=V_{of}/E$, $b=V_a/E$, $\omega=2\pi v\sqrt{LC}$ and $a-|b|/2>1$. Hence, the key point is in the selection of current references $\bar{x}_1(t)$, $\bar{x}_3(t)$ and a control law in such a way that the closed-loop system is stable and, at the same time, the output voltage scaled variable $x_o(t)$ converges to $\bar{x}_o(t)$ for $t\to+\infty$.

Assumption A. The nominal reference signals $\bar{x}_1$, $\bar{x}_3$, are smooth and T-periodic, with $\bar{x}_1^2(t)+\bar{x}_3^2(t)\neq 0$.

The control law $u=(u_1,u_2)^\top$ is selected as a Lyapunov-based state feedback action with components:

$$\begin{aligned}u_1 &= \bar{u}_1+\gamma(\bar{x}_2x_1-\bar{x}_1x_2),\\ u_2 &= \bar{u}_2+\gamma(\bar{x}_4x_3-\bar{x}_3x_4),\end{aligned} \tag{6}$$

where $\gamma>0$ and $\bar{u}=(\bar{u}_1,\bar{u}_2)^\top$ is the nominal control action

$$\bar{u}_1=\frac{1-\lambda_L\bar{x}_1-\dot{\bar{x}}_1}{\bar{x}_2}, \quad \bar{u}_2=\frac{1-\lambda_L\bar{x}_3-\dot{\bar{x}}_3}{\bar{x}_4}, \tag{7}$$

which is well defined under Assumption A.

Let $e_i=x_i-\bar{x}_i$, $i=1,2,3,4$, be the error variables. Then, the closed-loop error dynamics corresponding to Equations (4)–(6) is governed by the T-periodic system

$$\dot{e}=f(t,e)+g(t), \tag{8}$$

where

$$f(t,e)=[A(t)+B(\bar{u}(t))]e+\gamma B[u(t,e)-\bar{u}(t)]e \tag{9}$$

and

$$A(t)=\begin{pmatrix}-\lambda_L-\gamma\bar{x}_2^2(t) & \gamma\bar{x}_1(t)\bar{x}_2(t) & 0 & 0\\ \gamma\bar{x}_1(t)\bar{x}_2(t) & -\lambda-\gamma\bar{x}_1^2(t) & 0 & \lambda\\ 0 & 0 & -\lambda_L-\gamma\bar{x}_4^2(t) & \gamma\bar{x}_3(t)\bar{x}_4(t)\\ 0 & \lambda & \gamma\bar{x}_3(t)\bar{x}_4(t) & -\lambda-\gamma\bar{x}_3^2(t)\end{pmatrix},$$

while $B(\cdot)$ is a linear, skew-symmetric operator that acts on $\mathbb{R}^2$ vectors as follows:

$$B(v)=B(v_1,v_2)=\begin{pmatrix}0 & -v_1 & 0 & 0\\ v_1 & 0 & 0 & 0\\ 0 & 0 & 0 & -v_2\\ 0 & 0 & v_2 & 0\end{pmatrix}.$$

Moreover, $g(t)=(g_1(t),\ldots,g_4(t))^\top$, with $g_1(t)=g_3(t)=0$ and

$$g_2(t)=\frac{F_1(\bar{x}_1,\bar{\phi}_1(t))}{\bar{x}_2(t)}=\frac{\bar{x}_1(1-\lambda_L\bar{x}_1-\dot{\bar{x}}_1)-\bar{\phi}_1(t)}{\bar{x}_2(t)}, \tag{10}$$

$$g_4(t)=\frac{F_3(\bar{x}_3,\bar{\phi}_3(t))}{\bar{x}_4(t)}=\frac{\bar{x}_3(1-\lambda_L\bar{x}_3-\dot{\bar{x}}_3)-\bar{\phi}_3(t)}{\bar{x}_4(t)}, \tag{11}$$

DOI: 10.1002/cta

where

$$\bar{\phi}_1(t) = \bar{x}_2(t)[\dot{\bar{x}}_2(t) + \lambda(\bar{x}_2(t) - \bar{x}_4(t))], \tag{12}$$

$$\bar{\phi}_3(t) = \bar{x}_4(t)[\dot{\bar{x}}_4(t) + \lambda(\bar{x}_4(t) - \bar{x}_2(t))]. \tag{13}$$

Notice that Equation (8) may be regarded as a nominal T-periodic system, with an equilibrium point at $e=0$, affected by a T-periodic perturbation $g(t)$

$$\dot{e} = f(t, e) + \mu\hat{g}(t), \tag{14}$$

where $\mu = \|g(t)\|$ and $\hat{g}(t)$ is a unitary vector (in the sense of the uniform norm) in the direction of $g(t)$. The stability features of the nominal system, i.e. with $\mu=0$, will allow us to prove that, for a small enough μ, Equation (8) has a nontrivial, asymptotically stable periodic orbit which, in the large, has order $\|g(t)\|$.

Lemma 1
Let Assumption A be fulfilled. The equilibrium point $e=0$ of the T-periodic, nominal system

$$\dot{e} = f(t, e) \tag{15}$$

is:

(i) Exponentially stable in the linear approximation.
(ii) Globally uniformly asymptotically stable.

Proof
Using Equation (9), system (15) reads as

$$\dot{e} = [A(t) + B(\bar{u}(t))]e + \gamma B[u(t, e) - \bar{u}(t)]e \tag{16}$$

and its linear approximation in a neighborhood of $e=0$ is

$$\dot{e} = [A(t) + B(\bar{u}(t))]e. \tag{17}$$

(i) Let $V(e) = 1/2e^\top e$ be a Lyapunov function candidate for Equation (17). Taking into account that $B(\cdot)$ is skew-symmetric, one obtains that

$$\dot{V}(t, e) = e^\top A(t)e.$$

Denote as Δ_i the principal minor of $A(t)$ with dimension $i \times i$; then, by Assumption A

$$\Delta_1 = -\lambda_L - \gamma\bar{x}_2^2 \leqslant -\lambda_L < 0,$$

$$\Delta_2 = \lambda\lambda_L + \gamma(\lambda_L\bar{x}_1^2 + \lambda\bar{x}_2^2) \geqslant \lambda\lambda_L > 0,$$

$$\Delta_3 = -(\lambda_L + \gamma\bar{x}_4^2)\Delta_2 \leqslant -\lambda_L\Delta_2 < 0,$$

$$\Delta_4 = \lambda\lambda_L^2\gamma(\bar{x}_1^2 + \bar{x}_3^2) + \lambda_L\gamma^2\bar{x}_1^2(\lambda_L\bar{x}_3^2 + \lambda\bar{x}_4^2) + \lambda\lambda_L\gamma^2\bar{x}_2^2\bar{x}_3^2 \geqslant \lambda\lambda_L^2\gamma(\bar{x}_1^2 + \bar{x}_3^2) > 0$$

thus yielding the negative-definiteness of $A(t)$. Let now $\alpha_{\max}(t)$ denote the maximum eigenvalue of $A(t)$, which is trivially continuous and T-periodic, and let $\alpha_m < 0$ be defined as

$$\alpha_m = \sup\{\alpha_{\max}(t),\ t \in [0, T]\}.$$

Then, for all $e \neq 0$

$$\dot{V}(t, e) = e^\top A(t)e \leqslant \alpha_{\max}(t)\|e\|_2^2 \leqslant -|\alpha_m|\|e\|^2 < 0. \tag{18}$$

As $|\alpha_m|\|e\|^2$ is continuous and positive definite in $\mathbb{R}^4$ and it is also radially unbounded, it follows that $e=0$ is uniformly asymptotically stable [15]. Finally, for linear systems, as in Equation (17), uniform asymptotic stability and exponential stability are equivalent concepts [15].

DOI: 10.1002/cta

(ii) Using $V(e)=1/2e^{\top}e$ as a Lyapunov function candidate for Equation (16), it occurs again that $\dot{V}(t,e)=e^{\top}A(t)e$. From this point onwards the proof follows that of item (i). □

Proposition 2
Let Assumption A be fulfilled. Then, there exists an open neighborhood I_μ of $\mu=0$ such that, for each $\mu\in I_\mu$, the perturbed system (14) has one and only one exponentially stable, T-periodic solution $e(t,\mu)$ that verifies $e(t,0)=0$.

Proof
Under Assumption A, it is immediate from Equation (9) that f, $D_x f$, g and $D_x g$ are continuous with respect to all their arguments. Moreover, the variational system of the unperturbed equation (15) with respect to $e=0$ coincides with Equation (17), and Lemma 1.i indicates that Equation (17) does not have nontrivial T-periodic solutions and also that all its characteristic multipliers are in modulus less that 1. Hence, the thesis follows from Theorems 6.1.1 and 6.1.3 in [16]. □

Proposition 3
Let Assumption A be fulfilled. Then, for $t\to+\infty$ and for any positive constant $\theta<1$, the solution $e(t)$ of the perturbed system (8) satisfies

$$\|e(t)\|\leqslant\frac{\sqrt{2}}{|\alpha_m|\theta}\|g(t)\|. \tag{19}$$

Proof
It is known from Lemma 1.i that $e=0$ is an exponentially equilibrium point of the nominal error system (15). Moreover, the Lyapunov function $V(e)=1/2e^{\top}e$ for Equation (15) satisfies

$$\begin{aligned}
&c_1\|e\|^2=\tfrac{1}{2}\|e\|^2\leqslant V(e)=\tfrac{1}{2}\|e\|_2^2\leqslant\|e\|^2=c_2\|e\|^2,\\
&\dot{V}(t,e)\leqslant-|\alpha_m|\|e\|^2=-c_3\|e\|^2,\\
&\left\|\frac{\partial V}{\partial e}\right\|=\|e\|\leqslant\|e\|=c_4\|e\|,
\end{aligned}$$

for all $(t,e)\in[0,\infty)\times\mathbb{R}^4$. Furthermore, Assumption A guarantees that the perturbation term $g(t)$ is such that $\|g(t)\|=\delta<\infty$. Then, according to Lemma 9.2 in [15], there exists $t_0\in\mathbb{R}^+$ such that, for all $t\geqslant t_0$

$$\|e\|\leqslant\frac{c_4}{c_3}\sqrt{\frac{c_2}{c_1}}\frac{\delta}{\theta}=\frac{\sqrt{2}}{|\alpha_m|\theta}\|g(t)\|.$$

The usual control goal for system (4) is the tracking of *a priori* selected $\bar{x}_2$, $\bar{x}_4$, by the state variables x_2, x_4, respectively. Hence, whenever $\bar{x}_1$, $\bar{x}_3$ can be selected as T-periodic solutions of the Abel ODE [4] $F_i(\bar{x}_i,\bar{\phi}_i(t))=0$, $i=1,3$, i.e.

$$\bar{x}_i\left(1-\lambda_L\bar{x}_i-\dot{\bar{x}}_i\right)-\bar{\phi}_i(t)=0,\quad i=1,3, \tag{20}$$

fulfilling Assumption A, then $g(t)=0$ and Lemma 1 ensures the exact tracking target with global uniform asymptotic stability.

However, this is a challenging problem for which no theoretical results are still available. Ongoing research, still at a numerical stage, allows to conjecture the existence of periodic solutions for Equation (20) in particular situations that, unfortunately, do not satisfy Assumption A. This is due to the fact that, using Equation (5)

$$\dot{\bar{x}}_2(t)+\lambda[\bar{x}_2(t)-\bar{x}_4(t)]=-[\dot{\bar{x}}_4(t)+\lambda(\bar{x}_4(t)-\bar{x}_2(t))],$$

which makes $\bar{\phi}_1$, $\bar{\phi}_3$ to share zeros and, in turn, may force the nullifying of $\bar{x}_1$ and $\bar{x}_3$ at the same time instants according to Equation (20).

DOI: 10.1002/cta

The following section contains an HB-based proposal for the selection of periodic references $\bar{x}_1$, $\bar{x}_3$ in such a way that, besides satisfying Assumption A, $F_i(\bar{x}_i, \bar{\phi}_i)$, $i=1,3$ and, consequently, $g(t)$, are close to zero. Then, Propositions 2 and 3 guarantee locally exponentially stable T-periodic errors of order $\|g(t)\|$ in steady state.

3. HARMONIC BALANCE-BASED SELECTION OF CURRENT REFERENCES

Consider the set $L_2(0,T)$ of square integrable functions in $(0,T)$, provided with the usual scalar product $(\cdot\,|\,\cdot)$

$$(x(t)\,|\,y(t))=\frac{1}{T}\int_0^T x(t)y(t)\mathrm{d}t. \tag{21}$$

With the norm induced by Equation (21), $L_2(0,T)$ is a real, separable Hilbert space for which the *trigonometric system* $\{w_n\}_{n\geqslant 0}$, defined as

$$w_0=1,\quad w_{2n-1}=\sqrt{2}\cos n\omega t,\quad w_{2n}=\sqrt{2}\sin n\omega t \tag{22}$$

with $\omega=2\pi T^{-1}$ is a complete orthonormal system and, thus, a basis. Let also $X_N=\mathrm{span}\{w_0,\ldots,w_{2N}\}\subset L_2$ denote the subspace spanned by the $2N+1$ first elements of $\{w_n\}$. Then, the mapping $P_N: L_2\longrightarrow X_N$ acting on any $x\in L_2(0,T)$ as

$$P_N(x)=\sum_{n=0}^{2N}(x|w_n)w_n \tag{23}$$

is an orthogonal projection operator into X_N that allows $x\in L_2(0,T)$ to be uniquely decomposed as

$$x=P_N(x)+(\mathbb{I}-P_N)(x). \tag{24}$$

The selection of current references, $\bar{x}_1$, $\bar{x}_3$, is carried out according to the final discussion of Section 2. The HB method [4, 17] allows an Nth harmonic, T-periodic assignment $\bar{x}_{iN}(t)$ for $\bar{x}_i(t)$, $i=1,3$ to be found. For this, let us denote

$$\bar{x}_{iN}(t)=\alpha_{i0}+\sum_{n=1}^{N}\alpha_{in}\cos(n\omega t)+\beta_{in}\sin(n\omega t).$$

The proposal consists of obtaining the $2N+1$ unknown coefficients $\alpha_{i0},\ldots,\beta_{iN}$ solving the nonlinear system of $2N+1$ equations $P_N(F_i(\bar{x}_{iN},\bar{\phi}_i))=0$, equivalent to $(F_i(\bar{x}_{iN},\bar{\phi}_i)|w_n)=0$, $n=0,\ldots,2N$, i.e.

$$\int_0^T F_i(\bar{x}_{iN},\bar{\phi}_i)\cos(n\omega t)\mathrm{d}t=0,\quad n\in\{0,\ldots,N\}, \tag{25}$$

$$\int_0^T F_i(\bar{x}_{iN},\bar{\phi}_i)\sin(n\omega t)\mathrm{d}t=0,\quad n\in\{1,\ldots,N\}. \tag{26}$$

The next result studies the relation between the solutions $\bar{x}_{1N}$, $\bar{x}_{3N}$ of the HB equations (25)–(26), $i=1,3$.

Proposition 4
Assume that

$$x_{1N}(t)=\alpha_{10}+\sum_{n=1}^{N}\alpha_{1n}\cos(n\omega t)+\beta_{1n}\sin(n\omega t)$$

satisfies Equations (25)–(26) for $i=1$. Then

$$x_{3N}(t)=x_{1N}\left(t+\frac{T}{2}\right)=\alpha_{10}+\sum_{n=1}^{N}(-1)^n[\alpha_{1n}\cos(n\omega t)+\beta_{1n}\sin(n\omega t)]$$

satisfies Equations (25)–(26) for $i=3$.

DOI: 10.1002/cta

Proof
It is known by hypothesis that $P_N(F_1(\bar{x}_{1N}, \bar{\phi}_1))=0$, i.e.

$$P_N(\bar{x}_{1N}(1-\lambda_L\bar{x}_{1N}-\dot{\bar{x}}_{1N}))=P_N(\bar{\phi}_1(t)). \tag{27}$$

As it is immediate from Equations (12)–(13) and (5) that $\bar{\phi}_3(t)=\bar{\phi}_1(t+T/2)$, the evaluation of (27) in $t+T/2$ yields

$$P_N\left(\bar{x}_{1N}\left(t+\frac{T}{2}\right)\left[1-\lambda_L\bar{x}_{1N}\left(t+\frac{T}{2}\right)-\dot{\bar{x}}_{1N}\left(t+\frac{T}{2}\right)\right]\right)=P_N(\bar{\phi}_3(t))$$

and the result follows. □

When Equations (25)–(26) have solution for $i=1$, then Equation (24) allows writing

$$\begin{aligned} F_1(\bar{x}_{1N}, \bar{\phi}_1) &= P_N(F_1(\bar{x}_{1N}, \bar{\phi}_1))+(\mathbb{I}-P_N)(F_1(\bar{x}_{1N}, \bar{\phi}_1)) \\ &= (\mathbb{I}-P_N)(F_1(\bar{x}_{1N}, \bar{\phi}_1)). \end{aligned} \tag{28}$$

As a consequence, the function $g_{2N}(t)$ defined in (10) results in

$$g_{2N}(t)=\frac{(\mathbb{I}-P_N)(F_1(\bar{x}_{1N}(t), \bar{\phi}_1(t)))}{\bar{x}_2(t)}. \tag{29}$$

In turn, according to Equation (11), Proposition 4 and Equation (29), $g_{4N}(t)=g_{2N}(t+T/2)$, which means that $\|g_N(t)\|=\|g_{2N}(t)\|$. Therefore, an error bound may be calculated from Equation (19) in Proposition 3.

Remark 3.1
If $\|g_N(t)\|$ is small enough, Proposition 2 guarantees that the corresponding error Equation (14) has a T-periodic and asymptotically stable solution e_N. If it also happens that Equations (25)–(26) have a solution on increasing N and $\|g_N(t)\|\to 0$ for $N\to\infty$, one may expect that $\|e_N\|\to 0$ for $N\to\infty$.

The above described HB method provides trigonometric approximations $\bar{x}_{1N}, \bar{x}_{3N}$ for the current references for which the coefficients can only be obtained numerically. However, these coefficients depend on the converter parameters and, specifically, on the output resistance R through parameter λ (see (3)). Hence, if the converter undergoes piecewise constant load jumps, the performance will degrade until the disturbance is dynamically compensated by an appropriate modification of $\bar{x}_{1N}$, $\bar{x}_{3N}$ according to the actual value of R. This requires identification of R, solution of the new HB equations and updating of the current references. The time consumption associated with the second and third steps could be reduced if closed-form expressions $\bar{x}_{1N}(t, \lambda)$, $\bar{x}_{3N}(t, \lambda)$ were available. This is possible if one uses first harmonic HB approximations obtained from the ideal boost DC/AC system, that is, with no inductor loss resistances, which means $R_L=0$ and, consequently, $\lambda_L=0$ in Equations (25)–(26). Indeed, assuming

$$\bar{x}_1^{\mathrm{id}}(t, \lambda)=\alpha_{01}(\lambda)+\alpha_{11}(\lambda)\cos\omega t+\beta_{11}(\lambda)\sin\omega t \tag{30}$$

and taking into account that (recall Equation (12)–(2))

$$\bar{\phi}_1(t, \lambda)=\tilde{\alpha}_{01}(\lambda)+\sum_{n=1}^{2}\tilde{\alpha}_{n1}(\lambda)\cos(n\omega t)+\tilde{\beta}_{n1}(\lambda)\sin(n\omega t)$$

the solutions of Equations (25)–(26) with $\lambda_L=0$, that is, with

$$F_1(\bar{x}_1, \bar{\phi}_1)\equiv F_1^{\mathrm{id}}(\bar{x}_1^{\mathrm{id}}, \bar{\phi}_1)=\bar{x}_1^{\mathrm{id}}(1-\dot{\bar{x}}_1^{\mathrm{id}})-\bar{\phi}_1$$

are

$$\alpha_{01}=\tilde{\alpha}_{01}, \quad \alpha_{11}=\frac{\tilde{\alpha}_{11}+\omega\tilde{\alpha}_{01}\tilde{\beta}_{11}}{1+\omega^2\tilde{\alpha}_{01}^2}, \quad \beta_{11}=\frac{\tilde{\beta}_{11}-\omega\tilde{\alpha}_{01}\tilde{\alpha}_{11}}{1+\omega^2\tilde{\alpha}_{01}^2}. \tag{31}$$

DOI: 10.1002/cta

The function $g_2^{\mathrm{id}}(t,\lambda)$ is now

$$g_2^{\mathrm{id}}(t,\lambda)=\frac{F_1(\bar{x}_1^{\mathrm{id}}(t,\lambda),\bar{\phi}_1(t,\lambda)))}{\bar{x}_2(t)}=\frac{-\lambda_L(\bar{x}_1^{\mathrm{id}})^2+F_1^{\mathrm{id}}(\bar{x}_1^{\mathrm{id}},\bar{\phi}_1)}{\bar{x}_2}=$$
$$=\frac{-\lambda_L(\bar{x}_1^{\mathrm{id}})^2+(\mathbb{I}-P_1)[F_1^{\mathrm{id}}(\bar{x}_1^{\mathrm{id}},\bar{\phi}_1)]}{\bar{x}_2}. \tag{32}$$

Finally, it follows from Proposition 4 that

$$\bar{x}_{3N}^{\mathrm{id}}(t,\lambda)=\bar{x}_{1N}^{\mathrm{id}}\left(t+\frac{T}{2},\lambda\right)=\alpha_{01}(\lambda)-\alpha_{11}(\lambda)\cos\omega t-\beta_{11}(\lambda)\sin\omega t$$

and also that $g_4^{\mathrm{id}}(t,\lambda)=g_2^{\mathrm{id}}(t+T/2,\lambda)$.

Remark 3.2

In practical applications, real-time computation constraints make it difficult to implement controllers that include current references $\bar{x}_1$, $\bar{x}_3$ with more than two harmonics, i.e. with $N\geqslant 2$. In such cases, and also when using $\bar{x}_1^{\mathrm{id}}$, $\bar{x}_3^{\mathrm{id}}$, the voltages x_2, x_4 attain amplitudes presumably lower than expected. A possible solution to this issue might be to adjust the value of R_L, i.e. of λ_L, in the nominal control actions $\bar{u}_1$, $\bar{u}_2$ defined in Equation (7) till the output voltage amplitude reaches the desired value. Denoting as $\hat{\lambda}_L$ the adjusted value of λ_L eventually used in Equation (7), the corresponding perturbation terms $\hat{g}_{i+1N}(t)$, $i=1,3$ are

$$\hat{g}_{2N}(t)=\frac{\left(\lambda_L-\hat{\lambda}_L\right)\bar{x}_{1N}^2(t)}{\bar{x}_2(t)}+g_{2N}(t),\quad \hat{g}_{4N}(t)=\hat{g}_{2N}\left(t+\frac{T}{2}\right),$$

where $g_{2N}(t)$ is defined in Equation (29). When using the ideal approximations, $\hat{g}_2^{\mathrm{id}}$, $\hat{g}_4^{\mathrm{id}}$ follow straightforwardly replacing λ_L by $\hat{\lambda}_L$ in Equation (32).

However, the achievement of the correct output voltage amplitude is at the cost of a degradation of the sinusoidal shape of the signal, as shown in the simulation and experimental results.

4. SIMULATION RESULTS

The boost DC/AC converter used for simulation has parameters $E=8\ V$, $L=33\,\mu\mathrm{H}$, $C=1\,\mathrm{mF}$, $R=10\,\Omega$ and $R_L=0.19\,\Omega$, while $\gamma=0.00004$. For the output voltage references $\bar{V}_1$, $\bar{V}_2$ (recall Equation (2)), the selected offset and amplitudes are $V_{of}=20\ V$, $V_a=15\ V$, while $\nu=50\,\mathrm{Hz}$. Therefore, the expected output voltage is

$$V_o(\tau)=15\sin 100\pi\tau.$$

The simulations are carried out in real variables to allow a better comparison with the experimental results presented in Section 5.

The nominal current references $\bar{I}_{1N}$, $\bar{I}_{2N}$ have been obtained solving Equations (25)–(26) up to $N=5$ for $i=1$ and then using Proposition 4. On the one hand, the first row of Table I, as well as the fact that $V_{of}>|V_a|/2>E$, ensure the fulfillment of Assumption A. On the other hand, $\bar{I}_{1N}$, $\bar{I}_{2N}$, which are depicted in Figure 2, show convergence when increasing N. This is confirmed in Table I, where $\|g_N\|$ appears tending to 0.

The behavior of the boost DC/AC converter (1) under the control law (6)—converted to real variables—has been simulated for various sets of current references $\bar{I}_1$, $\bar{I}_3$ obtained according to the HB method introduced in Section 3. The system has been numerically solved with MAPLE using a Fehlberg fourth–fifth-order Runge–Kutta method with degree four interpolant. The initial conditions were $I_1(0)=I_2(0)=1$, $V_1(0)=V_2(0)=21$.

DOI: 10.1002/cta

Table I. Key features of current references, disturbance norms and simulated system response.

	$N=1$	$N=2$	$N=3$	$N=4$	$N=5$
$\inf\{\bar{I}_{1N}^2+\bar{I}_{2N}^2\}$	4.0120	0.0111	0.0116	0.0004	0.0002
$E\sqrt{C/L}\|g_N\|$	0.9940	0.2080	0.0680	0.0259	0.0107
$\|I_{1N}-\bar{I}_{1N}\|$	1.582	0.282	0.0949	0.0341	0.014
$\|V_{1N}-\bar{V}_1\|$	0.851	0.150	0.0481	0.0147	0.0057
$\|V_{oN}-\bar{V}_o\|$	0.6030	0.2390	0.0319	0.0234	0.0031

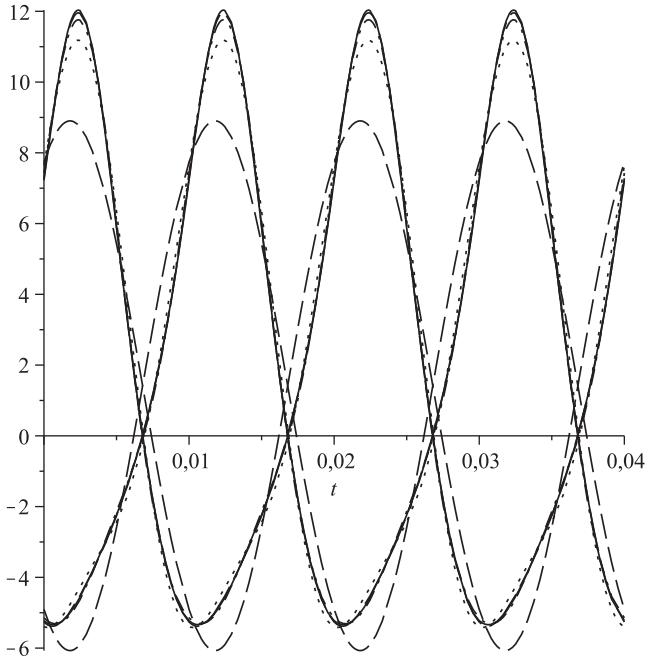

Figure 2. Nominal currents $\bar{I}_{1N}$, $\bar{I}_{2N}$ ($N=1$: dashed, $N=5$: solid).

Figure 3 portrays the output voltages V_{1N}, V_{2N}, $N=1,2$, obtained using the approximations $\bar{I}_{1N}$, $\bar{I}_{2N}$ in Equations (6)–(7), tracking the nominal voltage references $\bar{V}_1$, $\bar{V}_2$. The voltages corresponding to $N=3,4,5$ have not been included in the plot because they are almost indistinguishable amongst them and from $\bar{V}_1$, $\bar{V}_2$. Table I[‡] confirms again this information, because $\|I_{1N}-\bar{I}_{1N}\|$ and $\|V_{1N}-\bar{V}_1\|$ tend to 0. It is worth mentioning that the data corresponding to $\|I_{2N}-\bar{I}_{2N}\|$ and $\|V_{2N}-\bar{V}_2\|$ are omitted because they match exactly those of $\|I_{1N}-\bar{I}_{1N}\|$ and $\|V_{1N}-\bar{V}_1\|$, respectively. The output voltage variable $V_{oN}=V_{1N}-V_{2N}$ is depicted in Figure 4 together with the reference profile $\bar{V}_o$, for $N=1,2$. Notice that V_{oN} approaches $\bar{V}_o$ as N increases, confirmed by the last row in Table I.

Finally, the ideal current references $\bar{I}_1^{\mathrm{id}}$, $\bar{I}_2^{\mathrm{id}}$ have been computed from Equations (30)–(31). The obtained current references are such that $(\bar{I}_1^{\mathrm{id}})^2+(\bar{I}_2^{\mathrm{id}})^2=0.9888$, the fulfillment of Hypothesis A being thus guaranteed. Figure 5 portrays the output voltages V_o^{id} and $\hat{V}_o^{\mathrm{id}}$, the latter obtained according to Remark 3.2 with $\hat{R}_L=0.25\ \Omega$. Notice the shape degradation of $\hat{V}_o^{\mathrm{id}}$ pointed out in Remark 3.2.

[‡]The norm measures involving I_{1N}, V_{1N} and V_{oN} are in the steady state.

DOI: 10.1002/cta

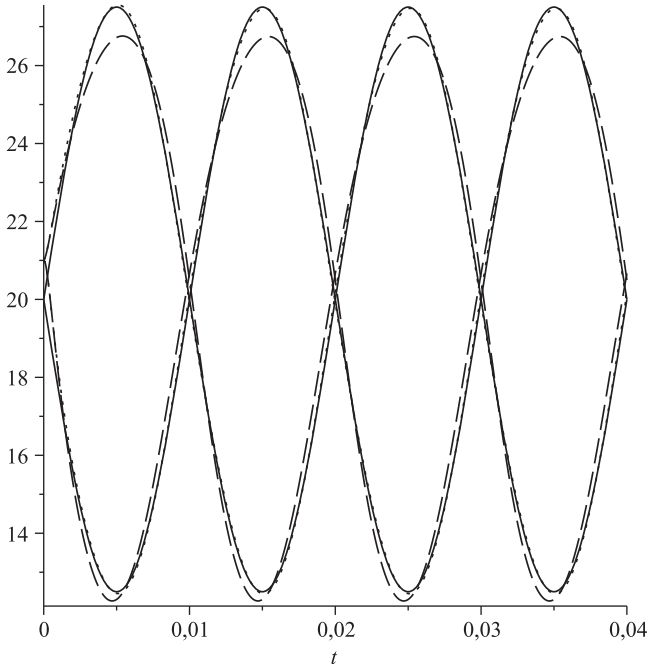

Figure 3. Voltages V_{1N}, V_{2N} ($\bar{V}_1$, $\bar{V}_2$: solid; $N=1$: dashed, $N=2$: dotted).

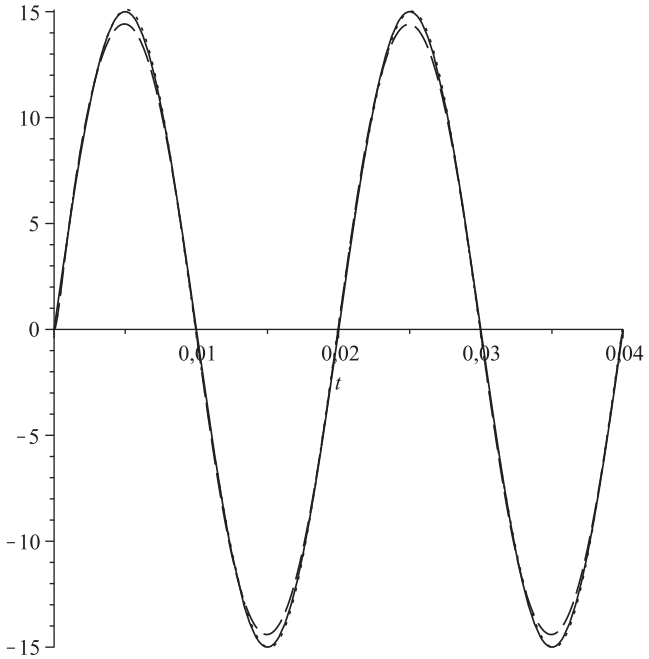

Figure 4. Output voltage V_{oN} ($\bar{V}_o$: solid; V_{o1}: dashed, V_{o2}: dotted).

5. EXPERIMENTAL RESULTS

The experimental results have been obtained by means of a prototype with the same parameter values used in the simulations of Section 4. Recall that the step-up conversion operation uses an input dc voltage source of 8V and delivers an output ac signal with an amplitude of 15V. However,

DOI: 10.1002/cta

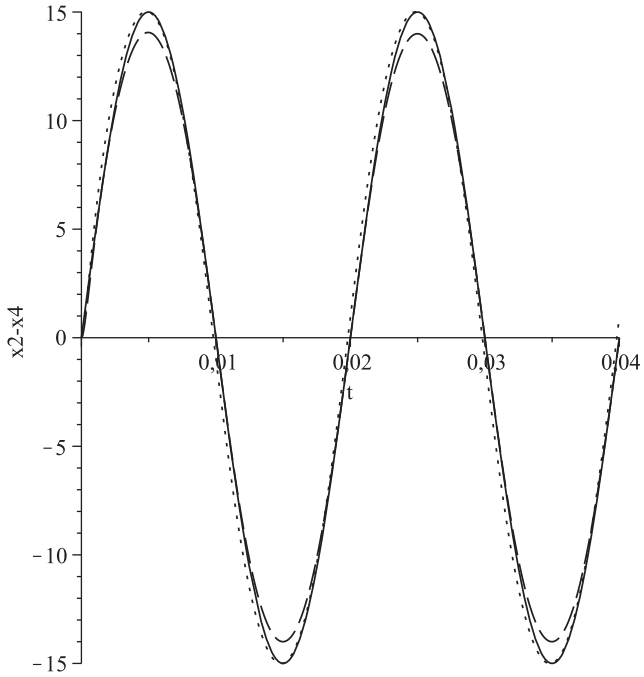

Figure 5. Output voltages V_o^{id}, $\hat{V}_o^{\mathrm{id}}$—without/with tuning of R_L in the control law—($\bar{V}_o$: solid; V_o^{id}: dashed; $\hat{V}_o^{\mathrm{id}}$: dotted).

it has to be pointed out that other conversion gains (step-up and step-down) have been tested in the laboratory.

The implementation has been carried out using two interconnected boost circuits with floating load. The prototype uses Eupec IGBT BSM 200 GB 170 DLC transistors which, due to the fact that there are currents flowing in opposite directions, they work in complementary mode. As the load does not have ground connection, the output voltage measures are differentially made between its extremes. Moreover, current and voltage sensor devices have been introduced for inductors and capacitors, respectively, in such a way that one has access to the four states of the converter. The controller is implemented by an algorithm in the digital signal processor AD21991, which includes the current references equations and generates the PWM signal for both IGBTs. The switching frequency is set to 13.5 kHz. It is also worth remarking that the prototype has been constructed to experimentally validate the theoretical predictions derived in the paper. Hence, its design does not answer to the usual optimization criteria in terms of efficiency, weight and size. Instead, the priority has been to simplify the digital implementation of the controller, this being achieved using a large capacitor that ensures a slow enough transient response.

Figure 6 contains a block diagram scheme detailing the control implementation. The control design stage involves the following steps:

1. Calculation (offline) of the inductor current references $(\bar{I}_1, \bar{I}_2)$ from the desired voltage references $(\bar{V}_1, \bar{V}_2)$ applying the HBM, as detailed in Section 3.
2. Obtention of the nominal control actions $(\bar{u}_1, \bar{u}_2)$ (see (7)) which, in the original variables, answer to:

$$\bar{u}_1 = \frac{E - R_L \bar{I}_1 - L\dot{\bar{I}}_1}{\bar{V}_1}, \quad \bar{u}_2 = \frac{E - R_L \bar{I}_2 - L\dot{\bar{I}}_2}{\bar{V}_2}.$$

3. Implementation of the control algorithm in the DSP:
   3.1. Measure of the inductor currents (I_1, I_2) and the capacitor voltages (V_1, V_2).

DOI: 10.1002/cta

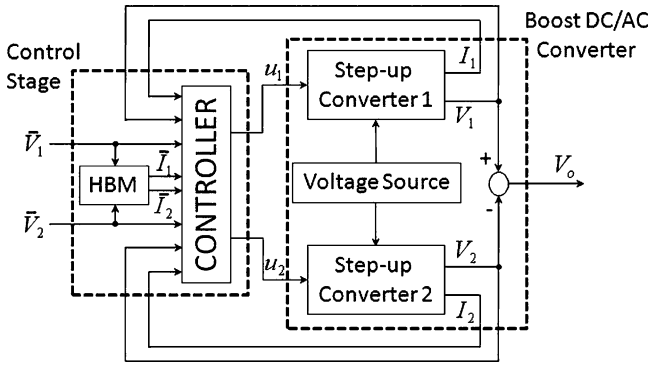

Figure 6. Block diagram detailing the control implementation.

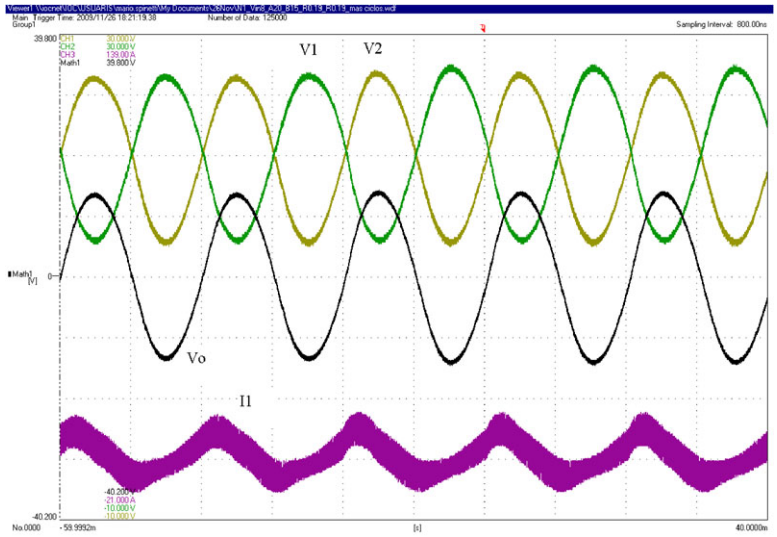

Figure 7. Experimental results with current references $\bar{I}_{11}$, $\bar{I}_{21}$, i.e. with one harmonic. V_1, V_2, V_o: [10V/div]; I_1: [20A/div].

3.2. Computation of the control actions $(\bar{u}_1, \bar{u}_2)$ (see (6)) which, in the original variables, answer to:

$$u_1 = \bar{u}_1 + \gamma(\bar{V}_1 I_1 - \bar{I}_1 V_1), \quad u_2 = \bar{u}_2 + \gamma(\bar{V}_2 I_2 - \bar{I}_2 V_2).$$

Figures 7, 8, 9 and 10 depict experimental measures of the capacitor voltages V_1 and V_2, the differential output voltage $V_o = V_1 - V_2$ and the inductor current $\bar{I}_1$, for different current references. Figures 7 and 8 use, respectively, current references with one and two harmonics, i.e. $\bar{I}_{1N}$, $\bar{I}_{2N}$ with $N = 1$ and $N = 2$. Figure 9 uses ideal current references $\bar{I}_1^{\mathrm{id}}$, $\bar{I}_2^{\mathrm{id}}$ with $R_L = 0.19\ \Omega$ in the control law, while Figure 10 also uses ideal expressions but with adjusted $\hat{R}_L$ in the control law according to Remark 3.2, i.e. with $\hat{R}_L = 0.26$.

The experimental data are in good agreement with the simulation results of Section 4 and, therefore, confirm the theoretical predictions. The inductor currents in Figures 7, 8 shape the nominal references in Figure 2, and the same happens between the experimental capacitor voltages of Figures 7, 8 and the simulated ones of Figure 3. The experimental output voltages are also in correspondence with the simulations: Figures 7 and 8 are to be compared with Figure 4, while Figures 9 and 10 are to be compared with Figure 5. For a better assessment of the results, Table II summarizes the main features of the output voltage responses obtained in simulation and experimentally for

DOI: 10.1002/cta

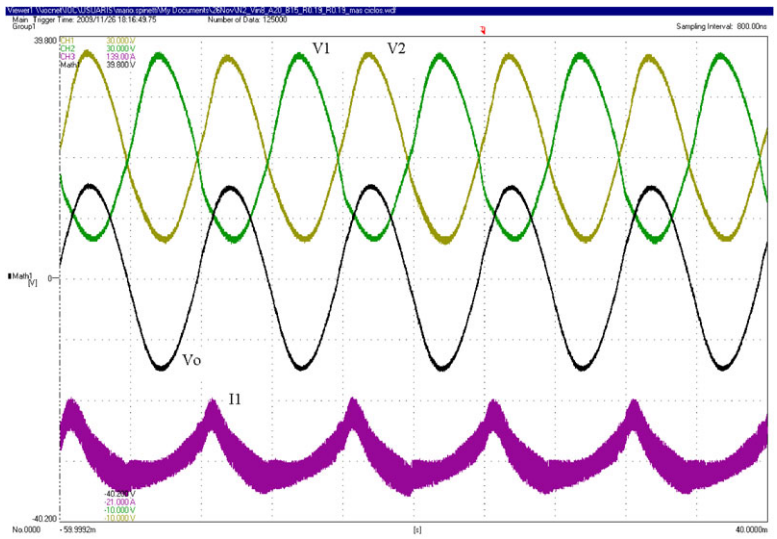

Figure 8. Experimental results with current references $\bar{I}_{12}$, $\bar{I}_{22}$, i.e. with two harmonics. V_1, V_2, V_o: [10V/div]; I_1: [20A/div].

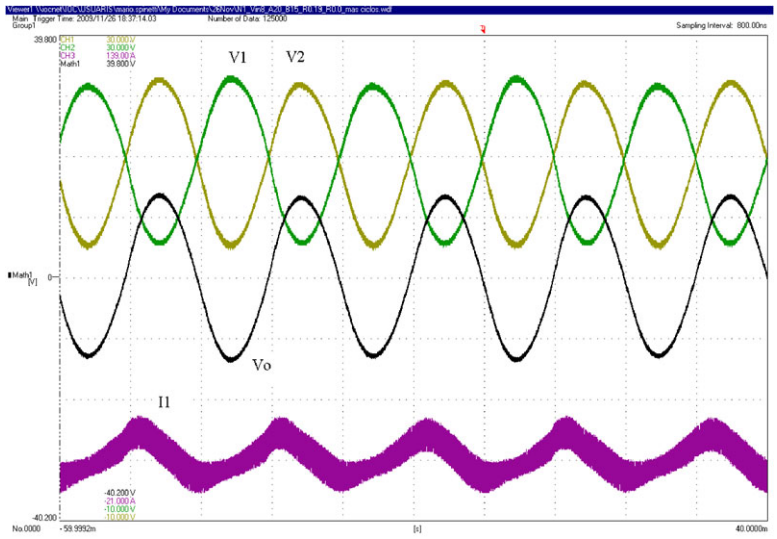

Figure 9. Experimental results with ideal current references $\bar{I}_1^{\mathrm{id}}$, $\bar{I}_2^{\mathrm{id}}$ and no adjustment of R_L in the control law. V_1, V_2, V_o: [10V/div]; I_1: [20A/div].

the different current references. Notice from the first two columns the performance improvement undergone by the boost DC/AC converter when using HB approximations with an increasing number of harmonics, namely, achievement of the desired Point-to-Point-Amplitude (PTPA) with THD reduction. The third and fourth columns show that the use of ideal, first harmonic HB references with adjusted $\hat{R}_L$ improves the PTPA at the cost of THD increasing, as discussed in Remark 3.2. Quantitative differences between experimental and simulated results are due to unmodelled internal resistances in the real plant, which cause lower voltage amplitudes. Indeed, when using ideal references with adjusted $\hat{R}_L$ in the control law, the simulation requires less $\hat{R}_L$ than the experimentation to attain the desired amplitude.

DOI: 10.1002/cta

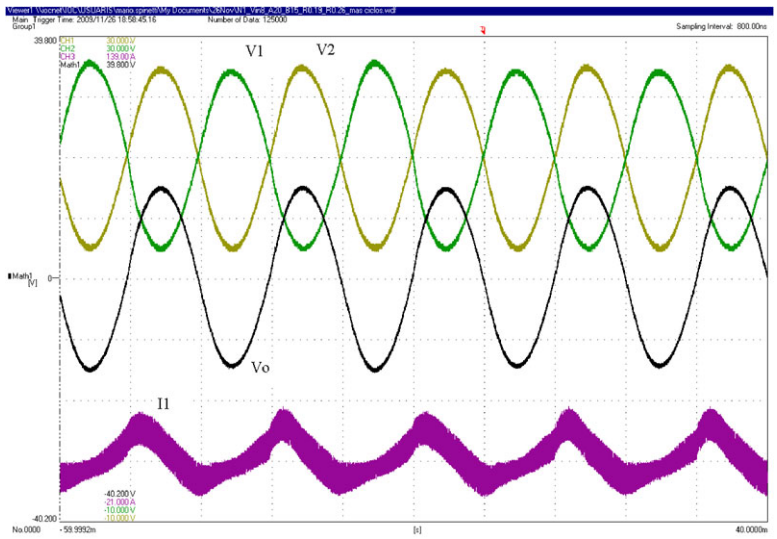

Figure 10. Experimental results with ideal current references $\bar{I}_1^{\mathrm{id}}$, $\bar{I}_2^{\mathrm{id}}$ and adjusted $\hat{R}_L = 0.26\,\Omega$ in the control law. V_1, V_2, V_o: [10V/div]; I_1: [20A/div].

Table II. Key features of experimental and simulation output voltage responses for different current references.

Experimental	$N=1$	$N=2$	$N=1$ (ideal)	$N=1$ (ideal, $\hat{R}_L=0.26$)
PTPA (V)	28	30	27	30
THD (%)	3	2.5	2.7	3.2
Simulated	$N=1$	$N=2$	$N=1$ (ideal)	$N=1$ (ideal, $\hat{R}_L=0.25$)
PTPA (V)	28.81	30.04	28	30.02
THD (%)	1.86	1.55	1.77	2.13

6. CONCLUSIONS AND SUGGESTIONS FOR FURTHER RESEARCH

This paper assesses the use of periodic current references in a Lyapunov-based controlled boost DC/AC converter under step-up inversion tasks. The results prove that, for sufficiently accurate current references, the system responds with asymptotically stable periodic solutions for which error bounds with respect to the expected behavior are provided.

The paper also propounds the use of HB-based techniques to obtain such current references. In case the HB approximations exist and converge, the theoretical results allow to expect that the output voltage error tends to zero. Otherwise, the proposed alternative is to use ideal, first-order HB approximations that are always obtainable and have an analytical, closed-form expression that depends explicitly on the converter parameters. The amplitude error problem that arises when using ideal HB approximations can be alleviated by an appropriate tuning of the control law parameters at the cost of slight THD increasing. Simulation and experimental results validate the study.

Further research should explore the possibilities offered by ideal first-order HB current references with regard to the attenuation of piecewise constant load disturbances by means of dynamic compensation.

ACKNOWLEDGEMENTS

The authors are grateful to the anonymous reviewers for their valuable comments and suggestions. This work is partially supported by the Spanish Ministerio de Educación under projects DPI2010-15110,

DOI: 10.1002/cta

DPI2008-01408 and DPI2010-14713-C03-03. J. M. Olm is also supported by the Spanish Ministerio de Ciencia e Innovación, through the Programa Nacional de Movilidad de Recursos Humanos of the Plan Nacional de $I-D+i$2008–2011.

REFERENCES

1. El Aroudi A, Rodríguez E, Orabi M, Alarcón E. Modeling of switching frequency instabilities in buck-based DC-AC H-bridge inverters. *International Journal of Circuit Theory and Applications* 2010, DOI: 10.1002/cta.627.
2. Zhang B, Zhou K, Wang Y, Wang D. Performance improvement of repetitive controlled PWM inverters: A phase-lead compensation solution. *International Journal of Circuit Theory and Applications* 2010; **38**(5):453–469.
3. Chu G, Tan SC, Tse CK, Wong SC. Robust current control for boost PFC converters from a sliding mode viewpoint. *International Journal of Circuit Theory and Applications* 2010, DOI: 10.1002/cta.661.
4. Zwillinger D. *Handbook of Differential Equations*. Academic Press: Boston, MA, 1993.
5. Fossas E, Olm JM. Asymptotic tracking in DC-to-DC nonlinear power converters. *Discrete and Continuous Dynamical Systems—Series B* 2002; **2**(2):295–307.
6. Cortés D, Álvarez Jq, Álvarez J, Fradkov A. Tracking control of the boost converter. *IEE Proceedings—Control Theory and Applications* 2004; **151**(2):218–224.
7. Sanchis P, Ursúa A, Gubía E, Marroyo L. Boost DC–AC inverter: a new control strategy. *IEEE Transactions on Power Electronics* 2005; **20**(2):343–353.
8. Cáceres RO, Barbi I. A boost dc–ac converter: analysis, design and experimentation. *IEEE Transactions on Power Electronics* 1999; **14**(1):134–141.
9. Vázquez N, Cortés D, Hernández C, Álvarez J, Arau J, Álvarez Jq. A new non-linear control strategy for the boost inverter. *Proceedings of the IEEE Power Electronics Specialist Conference*, Acapulco, Mexico, 2003; 1403–1407.
10. Hernández C, Vázquez N, Álvarez J, Arau J. Modified passive-based control law for the boost inverter. *Proceedings of the IEEE International Symposium on Industrial Electronics*, Rio de Janeiro, Brasil, 2003; 764–768.
11. Albea C, Gordillo F, Aracil J. Control of the boost DC–AC converter by energy shaping. *Proceedings of the 32nd IEEE Annual Conference of the IEEE Industrial Electronics Society*, Paris, France, 2006; 754–759.
12. Albea C, Canudas de Wit C, Gordillo F. Adaptive control of the boost DC–AC converter by energy shaping. *Proceedings of the 16th IEEE Conference on Control Applications*, Singapore, vol. 4, 2007; 611–615.
13. Calistan VA, Verghese GC, Stankovic AM. Multifrequency averaging of DC/DC converters. *IEEE Transactions on Power Electronics* 1999; **14**(1):124–133.
14. Wang F, Zhao H, Ma X. Analysis of slow-scale instability in boost PFC converter using the method of Harmonic Balance and Floquet theory. *IEEE Transactions on Circuits and Systems—I* 2010; **57**(2):405–414.
15. Khalil HK. *Nonlinear Systems* (3rd edn). Prentice-Hall Inc: Upper Saddle River, NJ, 2002.
16. Farkas M. *Periodic Motions*. Springer: New York, 1994.
17. Bonnin M. Harmonic Balance, Melnikov method and nonlinear oscillators under resonant perturbation. *International Journal of Circuit Theory and Applications* 2008; **36**(3):405–414.